IET Electric Power Applications

Research Article

IET Journals
The Institution of Engineering and Technology

Dynamic commutation torque-ripple reduction for brushless DC motor based on quasi-Z-source net

ISSN 1751-8660
Received on 15th April 2016
Accepted on 19th May 2016
doi: 10.1049/iet-epa.2016.0219
www.ietdl.org

Kun Xia[1,2] ✉, *Jing Lu*[1], *Chao Bi*[2], *Yuan Tan*[1], *Bin Dong*[1]

[1]*Department of Electrical Engineering, University of Shanghai for Science and Technology, Shanghai, People's Republic of China*
[2]*Department of Electrical and Computer Engineering, National University of Singapore, Singapore*
✉ *E-mail: galaxyx@sina.com*

Abstract: The commutation torque ripple in the six-step square-wave driving mode of the brushless DC motor affects the motor performance and generates mechanical vibrations and noise when used for industrial applications. The cause of commutation torque ripple is analysed in this study and a non-linear transient model of the phase current during the commutation interval is developed. According to the transient-current model, the commutation voltage and the time required to produce a constant torque can be calculated without current sampling; this makes the control system easier to realise in industrial applications, and reduces the need for a high performance controller. Based on the pulse-with modulated chopping method and quasi-Z-source net, the proposed control system can adjust the motor speed using a constant-voltage power supply and reduce the commutation torque ripple over the entire speed-adjustable range. A torque transducer is used to measure the dynamic torque ripple in the experiment. The results show that the proposed commutation torque-ripple reduction strategy can reduce the dynamic torque ripple by about 70% in both simulation and experiment compared with the traditional driving methods.

1 Introduction

The brushless DC motor (BLDCM) is widely used in industrial and domestic applications because of its high reliability, high power density, high torque to inertia ratio, simple structure, long life span, and easy-to-drive features [1, 2]. The performance of such motors has been significantly improved by the developments in power electronics, microelectronics, permanent magnet (PM) materials, and the control technology in the recent years [3–5].

However, torque ripple is the main drawback that limits the usable range of the BLDCM. An idealised BLDCM should have trapezoidal waveforms for back electromotive force (EMF), and can thus be fed with rectangular stator currents in a six-step square-wave driving mode. Since the motor windings are inductive, the controller cannot produce the ideal rectangular current during the commutation period, and a torque ripple is induced by current ripple during commutation. This kind of torque is defined as commutation torque ripple. The resulting torque ripple primarily affects the speed and accuracy of position control. It also induces mechanical vibrations and acoustic noise [6, 7].

Many control methods for reducing the commutation torque ripple have been developed in recent years. The authors in [8–10] presented some methods to reduce the commutation torque ripple using the three-phase pulse width modulation (PWM) technique. A new approach to optimise the current waveform based on the d q frame, which results in minimum torque ripple and maximum efficiency in BLDCM drives, was proposed in [11, 12]. However, the methods using the PWM technique can significantly reduce the commutation torque ripple at low speeds only.

For high speed operations, Shakouhi *et al.* [13] proposed a way to reduce the commutation torque ripple by energising the in-coming phase before the out-going phase switch-off. A method changing driving mode during commutation interval is illustrated in [14]. These methods increase the commutation time and have irregular phase current shapes. A DC–DC converter is used to compensate for the low of dc-link voltage during the commutation interval in [15, 16], which can significantly reduce the torque ripple at high speeds. A single-ended primary-inductor converter (SEPIC) circuit was introduced for adjusting the dc-link voltage during commutation in [17]. The SEPIC circuit drive system can reduce commutation torque ripple at both high and low speeds; however in [17], the phase resistance is neglected in order to simplify the control strategy which leads to lesser suppression of the torque ripples. Moreover, in reality the SEPIC circuit mostly operates in the boost mode most of the time.

In [18–21], several new methods that consider the effects of non-ideal back-EMF and minimise commutation time are discussed in depth. These methods help in constructing new models for motor driving system such as three-level neutral-point-clamped inverter with DC–DC converter and finite-state model predictive control.

The driving methods mentioned in these literatures using complex control methods with phase-current and DC-voltage measurements, or torque-estimation methods, to suppress the torque ripple. This makes the control methods difficult and expensive to realise in industrial applications. This paper propose a novel driving system based on the PWM-chopping method and lift converter which can significantly reduce the torque ripple in the entire speed-adjustable range without current sampling. The quasi-Z-source which has the advantage of large gain and high reliability [22] is employed to deal with the torque ripple at high speeds when power supply cannot provide enough dc-link voltage at commutation interval. The PWM technology is used to adjust the motor speed and reduce the commutation torque ripple at low speeds. The proposed method can also reduce the commutation torque ripple during changes in the speed or load in a timely and effective manner. The results of simulation and experiment show the reliability and efficiency of the driving system.

2 Torque ripple in BLDCM driving system

The torque ripple of the BLDCM is formed by three components: cogging torque, reluctance torque and mutual torque [23]. Cogging torque is a common shortcoming in PM motors, and can be minimised during motor design. PM motors with surface mounted

magnets do not demonstrate reluctance torque. In this paper, the reluctance and cogging torque have been neglected [24].

A typical equivalent circuit of BLDCM driving system is shown in Fig. 1*a*. U_{dc} is the dc-link voltage of the three phase voltage inverter. Equation (1) describes the voltage relations of the three-phase current during normal operation.

$$\begin{bmatrix} u_a \\ u_b \\ u_c \end{bmatrix} = \begin{bmatrix} R & 0 & 0 \\ 0 & R & 0 \\ 0 & 0 & R \end{bmatrix} \begin{bmatrix} i_a \\ i_b \\ i_c \end{bmatrix} + \begin{bmatrix} L & 0 & 0 \\ 0 & L & 0 \\ 0 & 0 & L \end{bmatrix} \frac{\mathrm{d}}{\mathrm{d}t} \begin{bmatrix} i_a \\ i_b \\ i_c \end{bmatrix} + \begin{bmatrix} e_a \\ e_b \\ e_c \end{bmatrix} + \begin{bmatrix} U_{N0} \\ U_{N0} \\ U_{N0} \end{bmatrix} \tag{1}$$

where, U_{N0} is the neutral point voltage; u_a, u_b, and u_c are the phase voltages; i_a, i_b, and i_c are the phase currents of A, B, and C phases; e_a, e_b, and e_c are the phase back-EMF; $L = L_S - M$ is the equivalent inductance of the phase windings, where, L_S is the self-inductance and M is the mutual inductance of individual coils; and R is the stator winding resistance.

Neglecting the cogging torque, the instantaneous electromagnetic (EM) torque can be expressed as

$$T_{em} = \left(e_a i_a + e_b i_b + e_c i_c\right) \frac{1}{\omega_r} \tag{2}$$

where, ω_r is the rotor speed. The dynamic equation of the motor can be expressed as

$$\frac{\mathrm{d}}{\mathrm{d}t}\omega_r = \frac{1}{J}\left(T_{em} - T_L - B\omega_r\right) \tag{3}$$

where B is the damping coefficient, J is the moment of inertia of the system, and T_L is the load torque.

From the EM torque equation, the sum of $e_a i_a$, $e_b i_b$, and $e_c i_c$ has to be constant in order to produce a constant EM torque. For the ideal 120° trapezoid back-EMFs, it can be observed that rectangular phase currents are required as shown in Fig. 1*b*, where P_A, P_B, and P_C represent the phases: A, B, and C, and H_a, H_b, and H_c represent the corresponding Hall signals for each phase. However, the ideal rectangular phase-current waveforms are hard to realise during the commutation process. The inductance of the stator winding impedes the change of phase current. Thus, the currents cannot fall to zero or increase to a constant value immediately after the commutation starts. Moreover the difference between the rising and falling rates of the current during the commutation period has a direct influence on the commutation torque.

The PWM-chopping method used in this paper, to adjust the BLDCM speed, is the PWM_ON scheme, which can minimise the commutation torque ripple compared with other switching modes [25]. The duty ratio of the PWM at a steady conduction state is D_0 while that during commutation interval is D_1.

In the following section, the commutation process of the current from phase AC to phase BC is analysed as an example. This current transfer is achieved by switching T_1 OFF and T_3 ON, with T_{42} remaining ON. For the existence of a stator induction, the current of the out-going phase A flows through the freewheeling diode of T_4 before falling to zero. The three phase voltages of the BLDCM can be expressed as

$$\begin{cases} 0 = Ri_a + L\dfrac{\mathrm{d}i_a}{\mathrm{d}t} + e_a + U_{N0} \\ U_{dc} \cdot D_1 = Ri_b + L\dfrac{\mathrm{d}i_b}{\mathrm{d}t} + e_b + U_{N0} \\ 0 = Ri_c + L\dfrac{\mathrm{d}i_c}{\mathrm{d}t} + e_c + U_{N0} \end{cases} \tag{4}$$

According to the instantaneous power theory, the neutral point U_{N0} can be written as

$$U_{N0} = (U_{dc} \cdot D_1 - e_a - e_b - e_c)/3 \tag{5}$$

To produce a constant torque, the rising and falling rates of the currents should be equal. That is

$$\frac{\mathrm{d}i_b}{\mathrm{d}t} = -\frac{\mathrm{d}i_a}{\mathrm{d}t} \tag{6}$$

After substituting and merging similar items, the PWM duty-ratio-D_1 during commutation can be illustrated as

$$U_{dc} \cdot D_1 = 3R\left(i_a + i_b\right) + e_a + e_b - 2e_c \tag{7}$$

When the back-EMF waveform of BLDCM is the ideal 120° trapezoidal (Fig. 1*b*), $e_a = E_m$, $e_b = E_m$, and $e_c = -E_m$ at the beginning of the commutation, where E_m is the amplitude of back-EMF, and it is expected to be constant during the commutation considering that the commutation interval is very

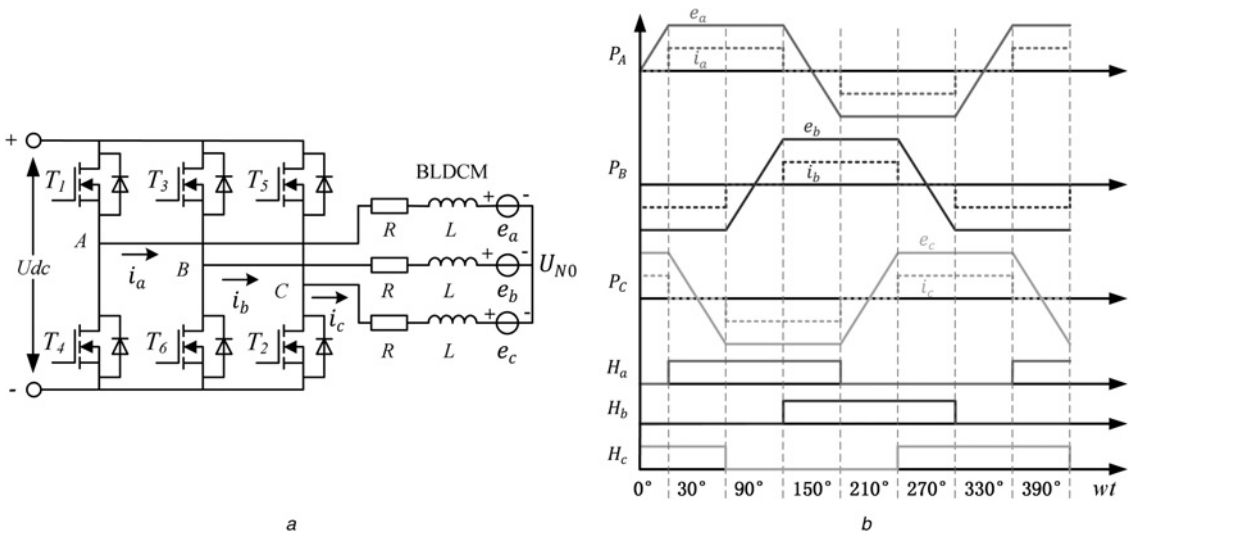

Fig. 1 *Conventional driving circuit and ideal back-EMF waveforms of the BLDCM*

a Inverter and equivalent circuit

b Ideal currents and back-EMFs with Hall signals

IET Electr. Power Appl., 2016, Vol. 10, Iss. 9, pp. 819–826

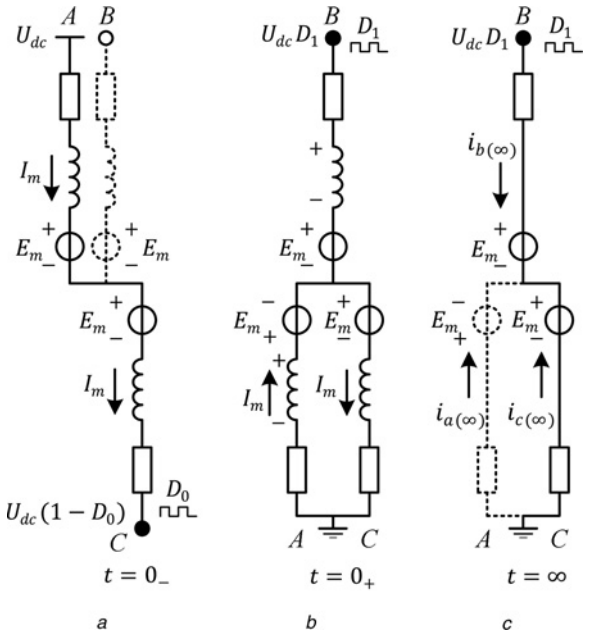

Fig. 2 *Driving system equivalent circuit during commutation interval*

a Before commutation start
b At the beginning of commutation
c Steady state of the circuit

short. Thus, the condition: $U_{\rm dc}\cdot D_1 = 3RI_m + 4E_m$, where I_m is the amplitude of the phase current, should be met to keep the rising and falling rates of the in-coming and out-going phase currents equal at the moment of commutation start.

The equivalent circuit of the BLDCM driving system during the commutation interval can be observed in Fig. 2. The steady state cannot be achieved in the driving system, since the phase A gets cut-off immediately when the current i_a falls to zero. At the beginning of commutation, the existing $i_{a(0-)} = (U_{\rm dc}\cdot D_0 - 2E_m)/2R$, $i_{b(0-)} = 0$ while $i_{a(\infty)} = -(U_{\rm dc}D_1 + 2E_m)/3R$, $i_{b(\infty)} = (2U_{\rm dc}D_1 - 2E_m)/3R$ at the steady statement and the discharge time constant $\tau = L/R$. The transient currents of the three phases i_a, i_b and i_c during the commutation interval before i_B falls to zero can be thus expressed as

$$\begin{cases} i_a = -\dfrac{U_{\rm dc}D_1 + 2E_m}{3R} + \left(\dfrac{U_{\rm dc}D_0 - 2E_m}{2R} + \dfrac{U_{\rm dc}D_1 + 2E_m}{3R}\right)\mathrm{e}^{-t/\tau} \\ i_b = \dfrac{2U_{\rm dc}D_1 - 2E_m}{3R} - \dfrac{2U_{\rm dc}D_1 - 2E_m}{3R}\,\mathrm{e}^{-t/\tau} \\ i_c = -\dfrac{U_{\rm dc}D_1 - 4E_m}{3R} - \dfrac{1.5U_{\rm dc}D_0 - U_{\rm dc}D_1 + E_m}{3R}\,\mathrm{e}^{-t/\tau} \end{cases} \tag{8}$$

From the above equation, the current fall time $t_{\rm f}$, which is the time taken by the current of the out-going phase to fall to zero, can be calculated as

$$t_{\rm f} = \frac{L}{R}\ln\frac{1.5U_{\rm dc}D_0 + U_{\rm dc}D_1 - E_m}{U_{\rm dc}D_1 + 2E_m} \tag{9}$$

Replacing i_a and i_b in (7) with the corresponding equations in (8), the commutation interval voltage required to produce a constant torque can be calculated as

$$U_{\rm dc}D_1 = 1.5U_{\rm dc}D_0 + E_m \tag{10}$$

This means that the falling and rising current rates would be equal, and that the torque ripple can be reduced by providing the required voltage expressed in (10) during the commutation interval. Then the current behaviours for different motor speeds can be found as shown in Figs. 3*b* and *c*, where $t_{\rm f}$ and $t_{\rm r}$ are the falling and rising times of the out-going and in-coming phases.

As shown in Fig. 3*c*, sometimes in high-speed situations, D_1 might be more than 1, but the duty ratio of the PWM cannot be greater than 1. To satisfy the requirement of a high pulsation voltage during the commutation interval, a quasi-Z-source net [26] and power-selection circuit are placed in front of the inverter. The output voltage of the quasi-Z-source net is set as the required commutation voltage, $U_{\rm dc}D_1$ ($D_1 > 1$). The power-selection circuit is used to shift the dc-link voltage from the power supply voltage to the quasi-Z-source output voltage at the start of commutation. The Commutation period can be calculated from (9), and the power-selection circuit would turn off at the end of commutation. Fig. 3*a* shows the proposed driving system for the BLDCM.

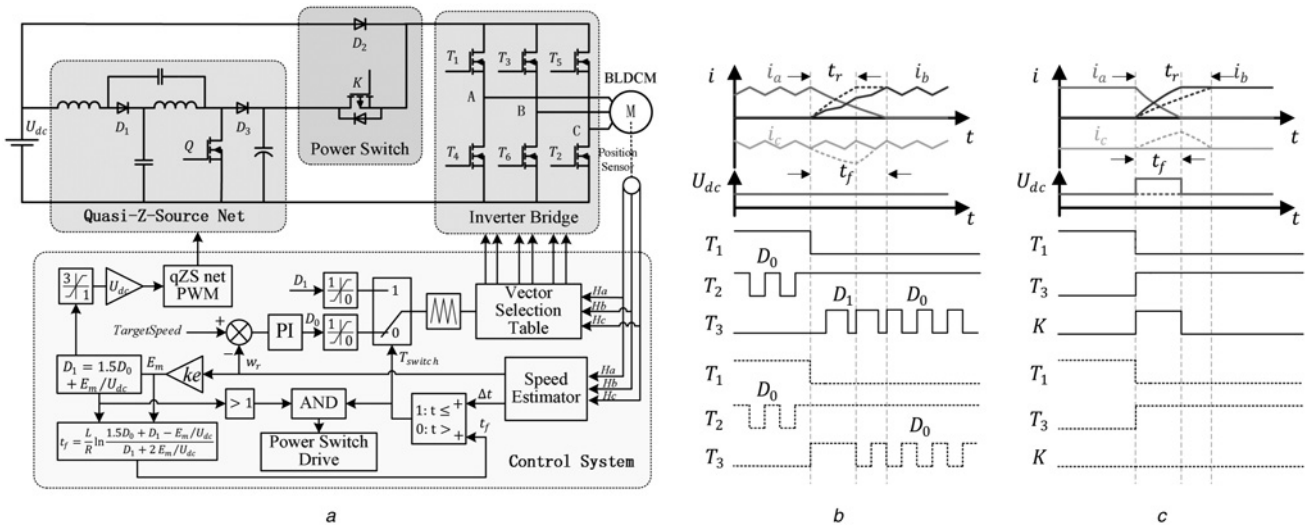

Fig. 3 *Configuration and switching patterns of BLDCM driving system with quasi-Z-source net*

a Configuration of BLDCM driving system
b Switching patterns at low speeds
c Switching patterns at high speeds

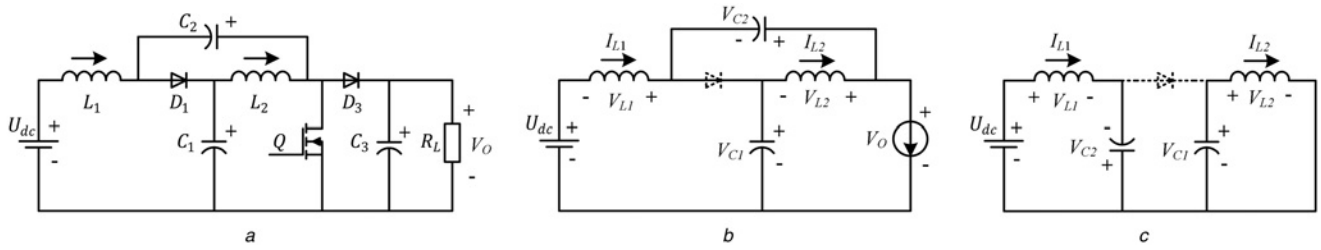

Fig. 4 *Operating state of quasi-Z-source net*

a Equivalent circuit of the quasi-Z-source net
b Non-shoot-through operating state
c Shoot-through operating state

Table 1 Switching states

Angle	T_1	T_2	T_3	T_4	T_5	T_6
30°	PWM	0	0	0	0	1
90°	1	PWM	0	0	0	0
150°	0	1	PWM	0	0	0
210°	0	0	1	PWM	0	0
270°	0	0	0	1	PWM	0
330°	0	0	0	0	1	PWM

1: Switch on, 0: Switch off, PWM: Switch on with PWM

When the motor is running at low speeds, such that D_1 is less than the 1, the duty ratio of the PWM is changed to maintain $U_{dc}D_1 = 1.5U_{dc}D_0 + E_m$ during the following commutation interval. Fig. 3*b* shows the switching states and phase-current waveforms during the commutation period in low speed operations. In this figure, the switch K, T_4, T_5, and T_6 are keeping off. At high speeds, a quasi-Z-source net is employed to provide a voltage higher than the DC power supply voltage, and the dc-link voltage is changed immediately at the beginning of every commutation interval using the power-selection circuit to ensure the equality constraint of the commutation voltage. Fig. 3*c* shows the current and dc-link voltage waveforms when the quasi-Z-source net is switched in the DC bus during the commutation interval at high speeds; T_4, T_5, T_6 are kept off while T_2 is on. The BLDCM can run at both low and high speeds with minimum torque ripple, if the proposed driving system is applied.

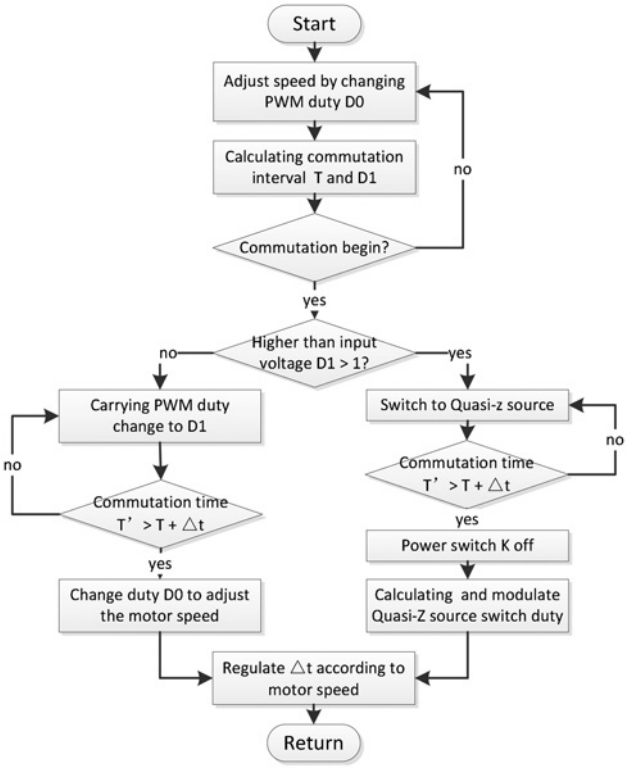

Fig. 5 *Flowchart of the proposed commutation control method*

3 Control strategy

As illustrated above, an adjustable commutation interval voltage is required to maintain $1.5U_{dc}D_0 + E_m$ to avoid the commutation torque ripple. At low speeds, the commutation input voltage can be decreased by changing the duty ratio of the PWM during the in-coming phase switches. When the motor runs at high speed, the quasi-Z-source net is employed to increase the dc-link voltage by adjusting the shoot-through ratio of the switch Q during the chopping cycle.

3.1 Quasi-Z-source net

The equivalent circuit of the quasi-Z-source net is shown in Fig. 4*a* [27]. U_{dc} is DC source voltage and R_L is the equivalent load of the driving system. The quasi-Z-source net can enhance the output voltage V_o, which appears at the load with the chopping of switch Q.

The two operating states of the quasi-Z-source net are the non-shoot-through operating state and the shoot-through operating state (Figs. 4*b* and *c*). In the non-shoot-through operating state, the switch Q is turned OFF, and the current is provided by the inductors L_1 and L_2 and the power supply U_{dc}. The capacitor C_1 stores, and the load consumes the energy; the diode D_1 operates like a wire in the ideal condition during its forward conduction. When the switch Q turns ON, the circuit works in the shoot-through state. The inductor L_1 in the left half of the circuit is charged by the energy released from the capacitor C_2 and the power supply U_{dc}, and the current of inductor L_1 increases. When the whole switching cycle is complete, the currents of the inductors L_1 and L_2 decrease again to supply energy to load. Eventually, V_o will be greater than U_{dc} and the voltage will be boosted.

The average output voltage of the quasi-Z-source net can be expressed as [28]

$$\bar{V}_o = \frac{1-D}{1-2D}U_{dc} \tag{11}$$

where, D is the duty ratio of the shoot-through period in one

Table 2 Parameters of the BLDCM driving system

Variable name	Value
rated voltage, V	24
rated power, W	42
rated speed, r/min	1000
pole pairs	2
phase resistance, Ω	0.75
phase inductance, mH	1.0368

IET Electr. Power Appl., 2016, Vol. 10, Iss. 9, pp. 819–826

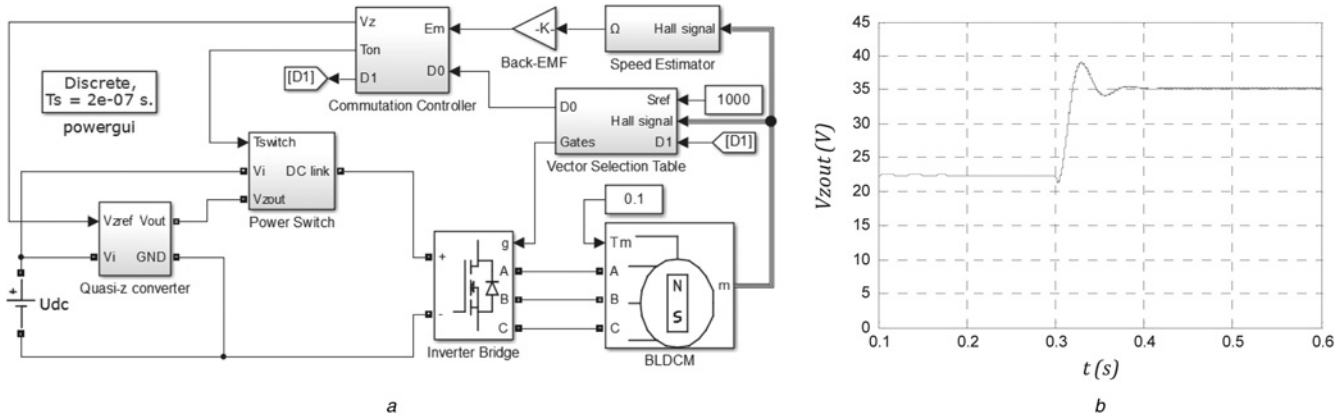

Fig. 6 *Simulation block diagram and output voltage characteristic*

a Simulation block diagram of the proposed driving system for BLDCM
b Output voltage adjustment characteristics of the quasi-Z-source net

switching cycle. The input DC power supply voltage can be boosted to an extremely high voltage with about 50% duty ratio. Thus, any required commutation interval voltage can be derived by changing the duty ratio of the switch Q in the high speed region.

Compared with the commutation interval, the adjusting process of the quasi-Z-source net takes a longer time (tens or hundreds of microseconds). Hence, the power selection circuit is required, and the switch K is employed to allow the DC bus to shift between the DC power supply and the quasi-Z-source net.

3.2 Control algorithm

During the commutation, the slopes of the in-coming phase currents are related to the commutation interval voltage $U_{dc}D_1$ and the maximum value of back-EMF E_m, where E_m is proportional to the motor speed and can be considered as a constant during commutation. The speed could be estimated from the Hall sensors of the BLDCM, and the required commutation voltage could be calculated from (10). The rising edges or falling edges of the Hall sensor signals, H_a, H_b, and H_c, as shown in Fig. 1*b*, are considered as the beginning of commutation. t_f, which is the time taken by the current of the out-going phase to fall to zero is considered as the period of the commutation interval. The principle driving strategy is a six-step square-wave driving method with voltage compensation during the commutation interval. Table 1 shows the switching states of the inverter according to the rotor positions.

The proposed topology for the BLDCM driving system and control strategy, realises minimum torque ripple in a wide speed

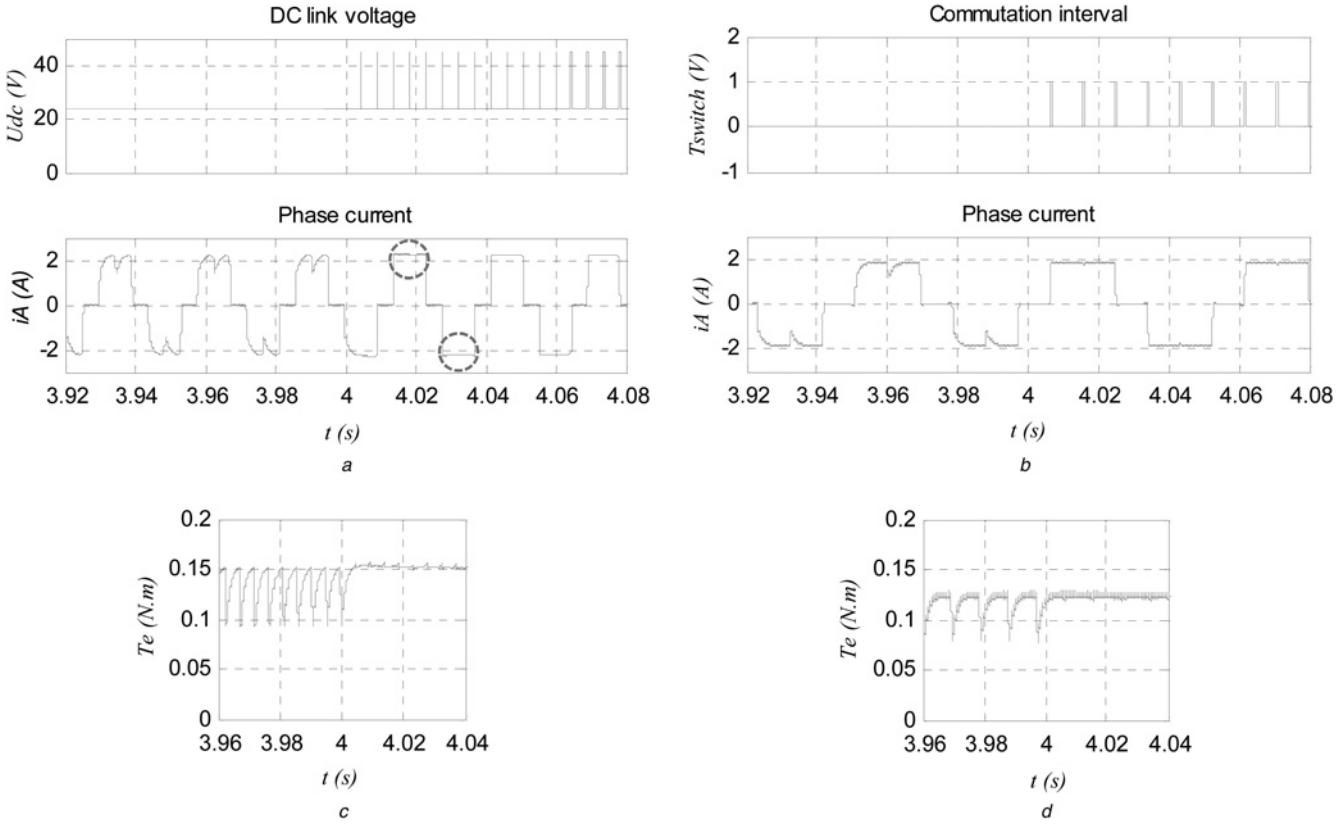

Fig. 7 *Simulation waveforms of the BLDCM*

a and *c* Current and torque waveforms, at high speeds (1000 r/min)
b and *d* Current and torque waveforms, at low speeds (500 r/min)

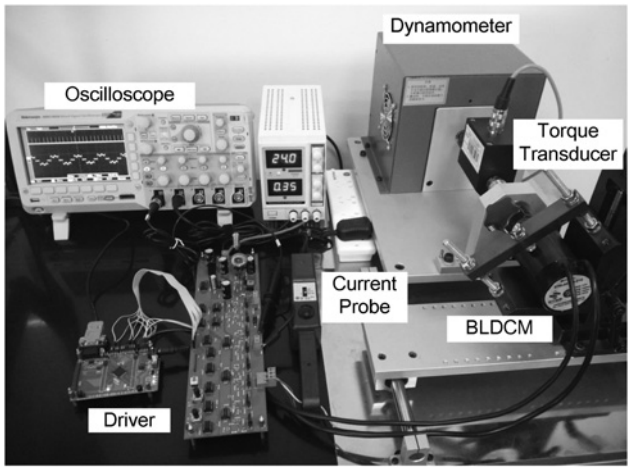

Fig. 8 *Experimental platform of BLDCM*

range. Before the beginning of commutation, the current falling time is calculated as the commutation interval T. The real commutation interval T' would increase when the motor speed changes. Thus, a Δt is used to correct the commutation time T when the motor speed changes, and it will be reset according to the value of the regulated speed. Then, the real commutation time can be calculated as $T' = T + \Delta t$. The flowchart of the proposed control strategy is shown in Fig. 5.

4 Simulation and experiment

Simulations and experiments were carried out to verify the feasibility of the proposed control strategy. The key parameters of the prototype motor, and their values, are shown in Table 2. The DC power supply used in the simulation and experiment was a 24 V constant-voltage source, and the frequencies of the PWM on the inverter and quasi-Z-source switches were 15 and 10 kHz, respectively.

4.1 Simulation results

The BLDCM driving system shown in Fig. 3*a* was constructed using MATLAB/Simulink. The overall block diagram of the proposed driving system of BLDCM is shown in Fig. 6*a*. The output voltage of the quasi-Z-source net is shown in Fig. 6*b*. The inductance and capacitance used in the quasi-Z-source net is 200 μH and 470 μF, respectively. The desired reference voltage of the quasi-Z-source net is set to 35 V at 0.3 s while the input voltage is 24 V. It is clear that the change of the output voltage from the input voltage of the DC power supply (U_{dc}) to the reference voltage, takes nearly 0.1 s. It is much longer than the commutation interval. Therefore, the power-selection circuit is employed in the driving system to switch the dc-link voltage between the DC power supply and the quasi-Z-source net output.

The simulation results of the BLDCM running at high (1000 r/min, rated speed) and low (500 r/min, half of rated speed) speeds with a constant load of 0.1 N·m are shown in Fig. 7. At high speeds, the steady conduction duty ratio D_0 of the PWM on the inverter is close to 100%; the dc-link voltage should be higher than the input voltage at the commutation interval to reduce the torque ripple, according to the proposed control strategy. In Fig. 7*a*, the dc-link voltage U_{dc} is switched to the quasi-Z-source net output, which has been regulated according to (10) at the commutation interval after 4 s. Comparing the BLDCM phase-current waveforms before and after 4 s, it is observed that the current fluctuations that contribute to the torque ripple are significantly reduced. The top and bottom of the phase-current waveforms are much smoother as indicated by the circles in Fig. 7*a*. When the BLDCM runs at low speeds, the ideal commutation voltage is much lower than the input DC power-supply voltage. The desired commutation voltage can be derived by changing the duty ratio of the PWM for the in-coming phase (Fig. 7*b*). The current ripple has also disappeared from the BLDCM phase-current waveform.

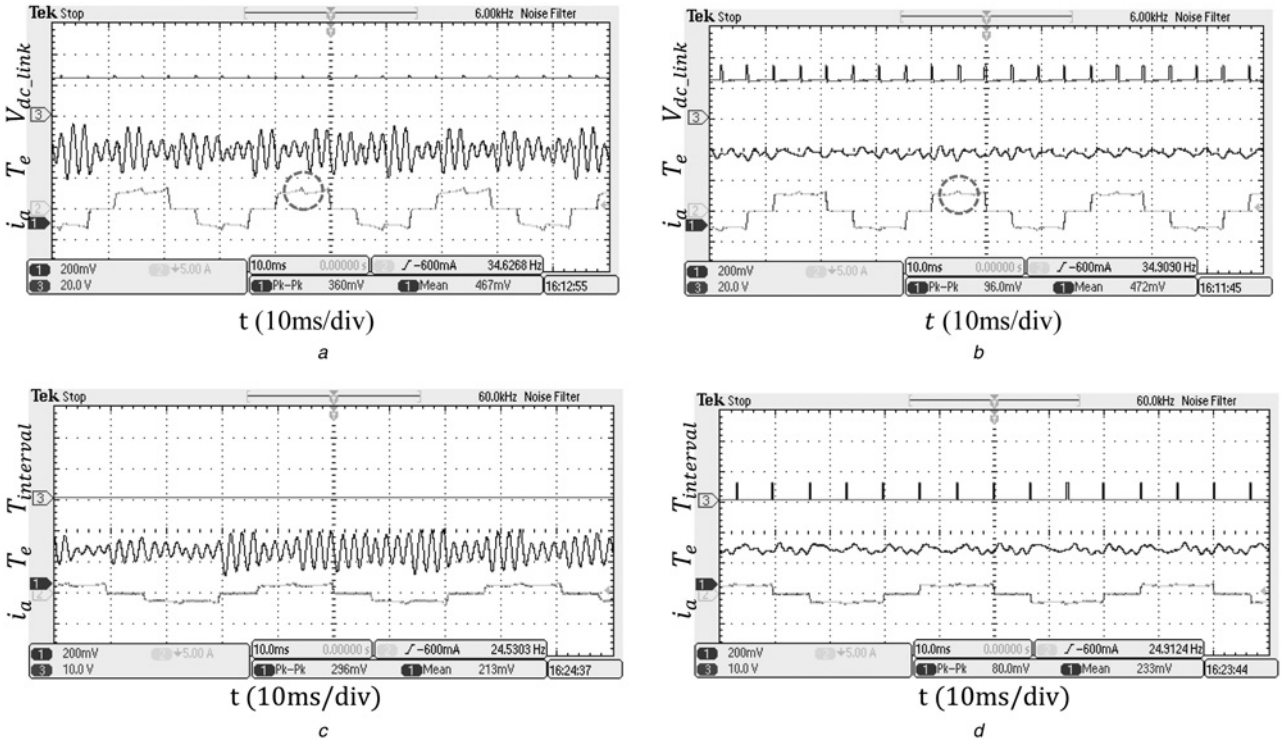

Fig. 9 *Experiment waveforms of BLDCM*

a and *c* Current and torque waveforms without and with the proposed control strategy at high speeds (1000 r/min)
b and *d* Current and torque waveforms without and with the proposed control strategy at low speeds (500 r/min)

IET Electr. Power Appl., 2016, Vol. 10, Iss. 9, pp. 819–826

The EM torque variations at high and low speeds are shown in Figs. 7*c* and *d*, respectively. When the proposed control strategy starts to work at 4 s, the torque ripple is significantly reduced under an appropriate commutation voltage. The torque ripple decreases by about 75%, from about 33.3% to 6.5%, at 1000 r/min, and from about 32.0% to 8.7% at 500 r/min. Moreover, the EM torque of the BLDCM has increased compared with the case without voltage compensation at high speeds. This is because of the extra power supplied from the quasi-Z-source net during the commutation interval.

4.2 Experiment results

The experiment platform of the proposed driving system for BLDCM is shown in Fig. 8. The main parameters of the BLDCM have already been presented in Table 2. The magnetic powder brake acts as the load. The core testing device is the high-precision non-contact shaft-to-shaft rotary torque sensor, TRS605, with 2-Mg N·m measurement accuracy and a 3-kHz sampling frequency. It connects the BLDCM and the brake with couplers for measuring the torque ripple precisely. The controller is based on a TMS320F28035 digital signal processor. The driver includes an inverter, quasi-Z-source net and power-selection circuit. The digital data acquisition system for the torque sensor and a Tek DPO5104 oscilloscope with a current probe A622 are the measurement instruments.

The testing results with and without the proposed torque ripple reduction strategy at high speeds (1000 r/min) are shown in Figs. 9*a* and *b*. Channel 1 provides the output voltage of the torque sensor. According to the data-sheet of the torque sensor, 0 to 5 V output voltage against 0 to 2 N·m torque can be expected. Channel 2 provides a one-phase current waveform. Channel 3 provides the dc-link voltage in Figs. 9*a* and *b* and the commutation interval in Figs. 9*c* and *d*. The phase current at the commutation interval, highlighted by a circle in Fig. 9*b*, is smoother than the phase current without the torque-ripple reduction shown in Fig. 9*a*. The torque ripple is reduced to 20.3% with the proposed control strategy, while the torque ripple of BLDCM with the traditional six-step square-wave control method reaches 77.1%.

The experiment waveforms with the same load at low speeds (500 r/min) are shown in Figs. 9*c* and *d*. It is obvious that the torque ripple is significantly reduced with the proposed control method, by about 75%, from 138.9% to 34.3%.

The torque ripple in one electric cycle of the BLDCM can be expressed in terms of the polar coordinates as shown in Figs. 10*a* and *b*. It is obvious that the characteristics of the output torque are improved greatly with the proposed driving strategy. For the limitations of motor manufacturing technology, the disadvantages of BLDCM, such as the non-ideal back-EMF, cogging torque, and deviation of Hall position contribute to the inherent torque ripple. Thus the dynamic torque ripple in the experiment is slightly larger than that in the simulation.

The real commutation interval T' can be adjusted dynamically when the load changes to adapt the changing parameters. When a 0.1 N·m load is applied suddenly to the output shaft of the normally running BLDCM, dynamic commutation torque-ripple reduction can be achieved along with the high response speeds for the control system. The experimental torque and current waveforms are shown in Fig. 10*c*.

5 Conclusion

This paper proposed control methods and a driving circuit for BLDCM, which could significantly reduce the commutation torque

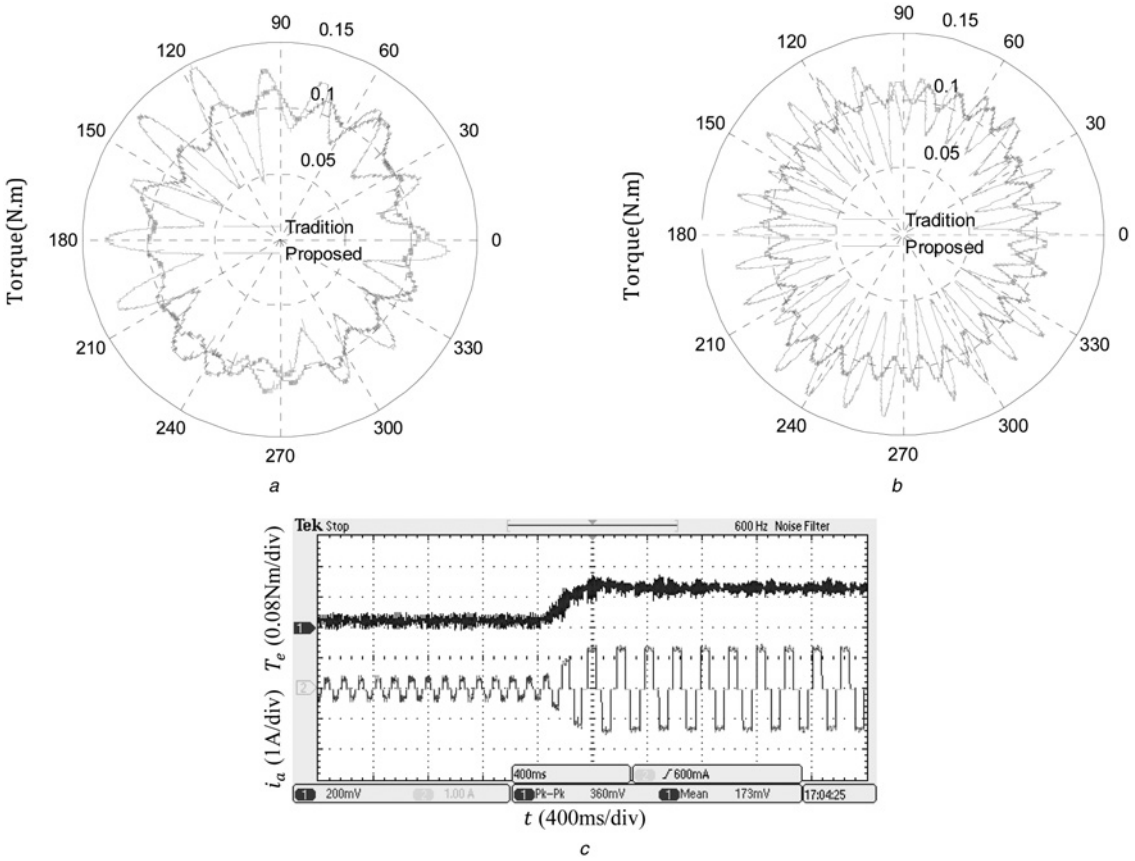

Fig. 10 *Experiment waveforms of BLDCM when the load changes*

a Comparison of the torque ripple with/without the proposed strategy at high speeds (1000 r/min)
b Comparison of the torque ripple with/without the proposed strategy at low speeds (500 r/min)
c Torque and current waveforms with the proposed control strategy

ripple over a large speed-adjustable range. Both simulations and experiments were performed, and the results showed the reliability and efficiency of the proposed control strategy. This driving method, if used in applications such as servo systems, electric bicycles, and fans, can result in better performances with lower vibrations and noise. In future research, the non-ideal back-EMF will be studied and a low-cost direct torque control will be realised.

6 Acknowledgment

This work was supported in part by the National Natural Science Foundation of China under grant no. 51207091.

7 References

1 Su, G.J., Mckeever, J.W.: 'Low-cost sensorless control of brushless DC motors with improved speed range', *IEEE Trans. Power Electron.*, 2004, **19**, (2), pp. 296–302
2 Son, Y.-C., Jang, K.Y., Suh, B.S.: 'Integrated MOSFET inverter module of low-power drive system', *IEEE Trans. Ind. Appl*, 2008, **44**, (3), pp. 878–886
3 Pan, C.T., Fang, E.: 'A phase-locked-loop-assisted internal model adjustable-speed controller for BLDC motors', *IEEE Trans. Ind. Electron.*, 2008, **55**, (9), pp. 3415–3425
4 Fang, J.Ch., Zhou, X.X., Liu, G.: 'Precise accelerated torque control for small inductance brushless DC motor', *IEEE Trans. Power Electron.*, 2013, **28**, (3), pp. 1400–1412
5 Rodriguez, F., Emadi, A.: 'A novel digital control technique for brushless dc motor drives', *IEEE Trans. Ind. Electron.*, 2007, **54**, (5), pp. 2365–2373
6 Bi, C., Jiang, Q., Lin, S., *et al.*: 'Reduction of acoustic noise in FDB spindle motors by using drive technology', *IEEE Trans. Magn.*, 2003, **39**, (2), pp. 800–805
7 Shakouhi, S.M., Mohamadian, M., Afjei, E.: 'Torque ripple minimization control method for a four phase brushless DC motor with non-ideal back-electromotive force', *IET Electr. Power Appl.*, 2013, **7**, (5), pp. 360–368
8 Lin, Y.K., Lai, Y.Sh.: 'Pulsewidth modulation technique for BLDCM drives to reduce commutation torque ripple without calculation of commutation time', *IEEE Trans. Ind. Appl.*, 2011, **47**, (4), pp. 1786–1793
9 Bharatkar, S.S., Yanamshetti, R., Chatterjee, D., *et al.*: 'Dual-mode switching technique for reduction of commutation torque ripple of brushless dc motor', *IET Electr. Power Appl.*, 2011, **5**, (1), pp. 193–202
10 Ziaeinejad, S., Sangsefidi, Y., Shoulaie, A.: 'Analysis of commutation torque ripple of BLDC motors and a simple method for its reduction'. Int. Conf. on Electrical Engineering and Informatics (ICEEI), Bandung, Indonesia, July 2011, pp. 1–6
11 Park, S.J., Park, H.W., Lee, M.H., *et al.*: 'A new approach for minimum-torque-ripple maximum-efficiency control of BLDC motor', *IEEE Trans. Ind. Electron.*, 2000, **47**, (1), pp. 109–114
12 Park, H.W., Park, S.J., Lee, Y.W., *et al.*: 'Reference frame approach for torque ripple minimization of BLDCM over wide speed range including cogging torque'. Proc. Int. Conf. IEEE ISIE, Pusan, Korea, June 2001, pp. 637–642
13 Shakouhi, S.M., Mohamadian, M., Afjei, E., *et al.*: 'Torque ripple minimisation control method for a fourphase brushless DC motor with non-ideal back-electromotive force', *IEEE Electr. Power Appl.*, 2013, **7**, (5), pp. 109–114
14 Ziyu, W., Haifeng, W., Guobiao, G., *et al.*: 'Torque ripple reduction in brushless DC motor drives'. ITEC Asia-Pacific, Beijing, China, 2014, pp. 1–4
15 Chen, W., Xia, C., Xue, M.: 'A torque ripple suppression circuit for brushless DC motors based on power DC/DC converters'. IEEE Third Int. Conf. on Industrial Electronics and Applications, Singapore, June 2008, pp. 1453–1457
16 Kun, X., Linling, Z., Yanneng, Z., *et al.*: 'Researches on the method of suppressing commutation torque ripple for brushless DC motors based on a Quasi-Z-Source net', *Proc. CSEE*, 2015, **35**, (4), pp. 971–978
17 Shi, T.N., Guo, Y.T., Song, P., *et al.*: 'A new approach of minimizing commutation torque ripple for brushless DC motor Based on DC–DC converter', *IEEE Trans. Ind. Electron.*, 2010, **57**, (10), pp. 3483–3490
18 Shi, J., Li, T.C.: 'New method to eliminate commutation torque ripple of brushless DC motor with minimum commutation time', *IEEE Trans. Ind. Electron.*, 2013, **60**, (6), pp. 2139–2146
19 Viswanathan, V., Jeevananthan, S.: 'Approach for torque ripple reduction for brushless DC motor based on three-level neutral-point-clamped inverter with DC–DC converter', *IET Power Electron.*, 2015, **8**, (1), pp. 47–55
20 Xia, Ch.L., Wang, Y.F., Shi, T.N.: 'Implementation of Finite-State model predictive control for commutation torque ripple minimization of permanent-magnet brushless DC motor', *IEEE Trans. Ind. Electron.*, 2012, **60**, (3), pp. 896–905
21 Ozturk, S.B., Toliyat, H.A.: 'Direct torque and indirect flux control of brushless DC Motor', *IEEE/ASME Trans. Mechatronics*, 2011, **16**, (2), pp. 351–360
22 Anderson, J., Peng, F.Z.: 'Four quasi-Z-source inverters'. Power Electronics Specialists Conf., IEEE PESC'08, Rhodes, June 2008, pp. 2743–2749
23 Niguchi, N., Hiratr, K.: 'Torque ripple analysis of a magnetic-geared motor'. ICEM, Marseille, France, September 2012, pp. 789–794
24 Xu, F.P., Tiecai, L., Tang, P.H.: 'A low cost drive strategy for BLDC motor with low torque ripples'. ICIEA, Singapore, June 2008, pp. 2499–2502
25 Zhou, M.L., Li, Zh., Gu, Q., *et al.*: 'Influence of PWM modes on non-commutation torque ripple in brushless DC motor control system'. Proc. Int. Conf. ICMIC. Measurement, Harbin, China, August 2013, pp. 16–18
26 Peng, F.Z., Joseph, A., JinWang, C., *et al.*: 'Z-source inverter for motor drives', *IEEE Trans. Power Electron.*, 2005, **20**, (4), pp. 857–863
27 Liu, H., Liu, P., Zhang, Y.: 'Design and digital implementation of voltage and current mode control for the quasi-Z-source converters', *IET Power Electron.*, 2013, **6**, (5), pp. 990–998
28 Liu, Y., Ge, B., Abu-Rub, H.: 'Theoretical and experimental evaluation of four spacevector modulations applied to quasi-Z-source inverters', *IET Power Electron.*, 2013, **6**, (7), pp. 1257–1269